Generation of seiches by cold fronts over the southern North Sea

M. P. C. de Jong, L. H. Holthuijsen, and J. A. Battjes
Environmental Fluid Mechanics Section, Delft University of Technology, Delft, Netherlands

Received 2 April 2002; revised 27 September 2002; accepted 28 January 2003; published 12 April 2003.

[1] Seiches affecting the Port of Rotterdam are generated in the Southern North Sea. Their generation is investigated with observations and numerical simulations. A wavelet analysis of the observations, both at sea and in the harbor, shows that low-frequency energy (0.1–2.0 mHz) does indeed occur at sea prior to each seiche event in Rotterdam. An analysis of 6 years of weather charts indicates that all 51 seiche events in this period (with amplitude exceeding 0.25 m) coincided with the passage of a low-pressure weather system. Some of these low-pressure systems included a sharp cold front (classical or ana), whereas others included a more diffuse cold front (split or kata). Numerical simulations with a hydrodynamic model driven by meteorological observations reproduced the seiches for situations with the sharp cold fronts correctly. The seiches that were simulated for situations with the gradual cold fronts do not agree with the observations, which is ascribed to the inadequate atmospheric forcing of the hydrodynamical model. *INDEX TERMS:* 4560 Oceanography: Physical: Surface waves and tides (1255); 4504 Oceanography: Physical: Air/sea interactions (0312); 4219 Oceanography: General: Continental shelf processes; *KEYWORDS:* cold fronts, generation of seiches, Port of Rotterdam, prediction of seiche events, seiches

Citation: de Jong, M. P. C., L. H. Holthuijsen, and J. A. Battjes, Generation of seiches by cold fronts over the southern North Sea, *J. Geophys. Res.*, *108*(C4), 3117, doi:10.1029/2002JC001422, 2003.

1. Introduction

[2] Due to supply of energy from open sea, standing waves can occur in harbor basins. Occasionally, the amplitude of these waves (also known as seiches) becomes abnormally large, apparently in response to changes in the energy supply from sea. This response of harbor basins is relatively well known [*Mei*, 1989]. However, the detailed mechanisms of the origin of the low-frequency energy are not well understood.

[3] Low-frequency energy at sea can be generated by a number of mechanisms, for example, surf beat, tsunamis, internal waves, and atmospheric disturbances [*Wilson*, 1972; *Giese and Chapman*, 1993; *Korgen*, 1995]. The dominating source may differ from harbor to harbor, depending on the occurrence of such mechanisms and the specific geographic situation of the harbor. The present study is aimed at the source of seiches in the Port of Rotterdam, Netherlands (Figure 1). Here, seiches occur mainly in the Calandkanaal (length ≈20 km, depth ≈20 m) with measured amplitudes up to 0.9 m (at Rozenburgse Sluis (ROZ), near the closed end of the Calandkanaal). For almost all of the observed seiches, the dominant frequency is the lowest eigenfrequency equivalent to a period of 90 min (somewhat dependent on the water depth which varies with the tide). A relatively small number of events has been observed in which the response at the second eigenfrequency is dominant (equivalent to 50 min). These observed frequencies agree with predictions by *Kernkamp* [1999], who showed that the lowest two eigenfrequencies of the Calandkanaal are approximately 0.19 mHz and 0.33 mHz.

[4] Atmospheric phenomena are the most probable cause of these seiches. This hypothesis is supported by the fact that all significant seiche events occur during the passage of low-pressure areas and cold fronts. The other potential generating mechanisms are either extremely rare near Rotterdam (e.g., tsunamis), or they do not generate energy near the eigenfrequencies of the harbor (e.g., surf beat).

[5] The generation of seiches by atmospheric disturbances has been studied earlier for Nagasaki Bay, Japan [*Hibiya and Kajiura*, 1982]. For this case, numerical simulations showed that a sudden increase ("jump") of 3 hPa (mbar) followed by a gradual decrease in pressure generated long waves at sea, subsequently causing the observed seiche.

[6] *Gomis et al.* [1993], *Garcies et al.* [1996], *Monserrat et al.* [1991a, 1991b], and *Rabinovich and Monserrat* [1996, 1998] studied seiches at the Ciutadella inlet of the Balearic Islands. They too found a high correlation between atmospheric pressure fluctuations and seiche intensity inside the inlet. *Vidal et al.* [2001] showed with numerical simulations, forced by observed pressure fluctuations, that these seiches are generated by a standing wave at sea between two of the Balearic Islands.

0148-0227/03/2002JC001422$09.00

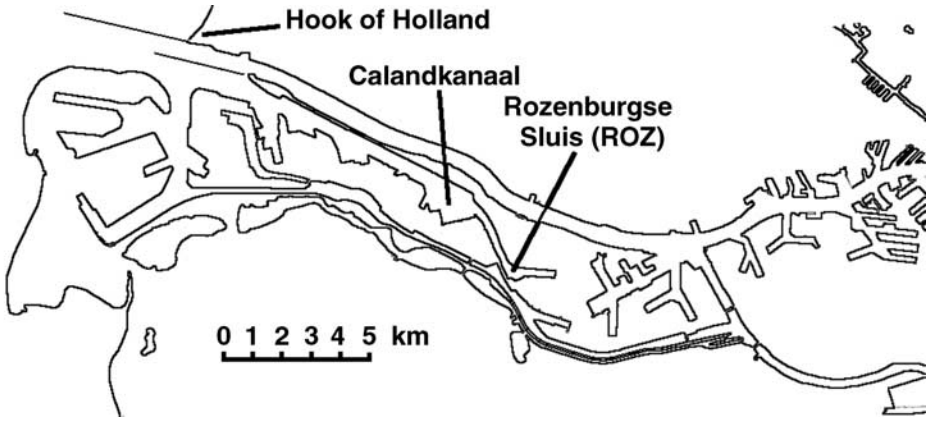

Figure 1. Port of Rotterdam.

[7] *Candela et al.* [1999] studied the atmospheric generation of seiches in harbors near the Strait of Sicily, Italy. These seiches were also found to coincide with the passage of low-pressure systems. However, numerical simulations driven by synthetic low-pressure systems (without cold front) did not reproduce the observed low-frequency energy at sea. In contrast to this, simulations with hypothetical atmospheric pressure jumps did produce seiches. These jumps were not measured and further observations are needed to confirm their occurrence.

[8] The possibility of meteorologically generated seiches in the Port of Rotterdam has been suggested for a long time [see, e.g., *Wemelsfelder*, 1957]. However, most previous studies of seiches in the Port of Rotterdam focused mainly on the phenomena inside the harbor [see, e.g., *de Looff and Veldman*, 1994; *Kernkamp*, 1999].

[9] The aim of the present work is to describe some typical (meteorological) observations during seiche events in the Port of Rotterdam and to analyze a potential meteorological origin for these events. To address the problem for the Port of Rotterdam, measurements of water levels, atmospheric pressure and wind have been obtained at a number of locations at sea and inside the harbor. These measurements are analyzed in this study with a wavelet technique. The generation of low-frequency energy at sea and the response of the harbor to this incoming energy is numerically simulated for two events.

2. Measurements

2.1. Data Acquisition

[10] Pertinent measurements obtained in the time interval 1995–2001 are used for this study. Surface elevation, wind speed and atmospheric pressure at sea were measured at Europlatform (EUR), Lichteiland Goeree (GOE) and Meetpost Noordwijk (MPN). Figure 2 shows the locations of these offshore platforms, all within 40 km from the harbor mouth.

[11] At one or more of these platforms, the surface elevation measurements (obtained with step gauges and radar altimeters) are available for one long period (5 consecutive winter months of 1996–1997) and for a few events in 1995, 2000 and 2001. The sample rate of the surface elevation measurements is 4 Hz (prior to 2000) or 2.56 Hz (2000 and later). Inside the harbor, surface elevation measurements are available from Rozenburgse Sluis (ROZ), located near the closed end of the Calandkanaal (see Figures 1 and 2). These measurements have been taken continuously since 1995 with a floater, sampled at a 60-s interval. Meteorological measurements (atmospheric pressure, wind speed and wind direction) were also available at the platforms at sea as 10-min-average values for the same time periods.

[12] Meteorological measurements at Hook of Holland (HOH) with a sampling interval of 10 min (Figures 1 and 2), consisting of average values based on 10 min centered around the time stamp, were used to analyze the meteorological situation during all seiche events in the period 1995–2000. In addition, wind speed, wind direction, atmospheric pressure, precipitation and air temperature are obtained continuously since January 2000 as one minute averages at Rotterdam Airport (RA, Figure 2).

2.2. Data Analysis

[13] For this study, seiche events are defined as episodes in which the seiche amplitude at ROZ exceeds 0.25 m. To identify these seiche events and the corresponding increased levels of low-frequency energy at sea, a wavelet analysis based on the Morlet wavelet [*Morlet et al.*, 1982] has been

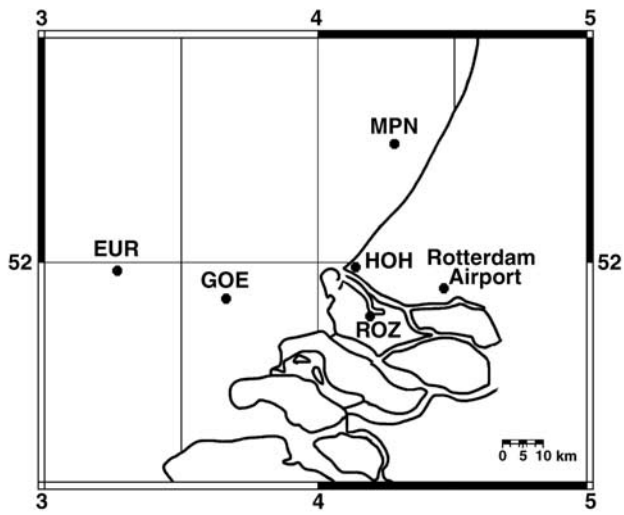

Figure 2. Hydro-meteo observations at platforms EUR, GOE and MPN at sea near the Port of Rotterdam.

applied to the entire surface elevation data set. This analysis technique transforms the original data from the time domain to the timescale (period) domain.

[14] The Morlet wavelet in terms of time domains t and t' and period T is given by

$$\psi(T,t,t') = e^{im\frac{t'-t}{T}} e^{-\left(\frac{t'-t}{T}\right)^2/2}, \quad (1)$$

in which m is a constant value, which needs to be larger than 5 to ensure zero mean of the wavelet (for this study $m = 6$).

[15] The wavelet transform $\hat{x}(T, t)$ of a time series $x(t')$ is then defined as the inner product of ψ and $x(t')$,

$$\tilde{x}(T,t) = \frac{1}{\sqrt{T}} \int_{-\infty}^{+\infty} x(t)\psi^*(T,t,t')dt', \quad (2)$$

in which the asterisk indicates the complex conjugate (see, for example, *Farge* [1992] and *Torrence and Compo* [1998] for a more comprehensive general descriptions of the wavelet transform).

[16] This transformation can be used to determine wavelet spectra defined as $W_x(T, t) = |\tilde{x}(T, t)|^2$. From these spectra, the occurrence of seiches or of low-frequency energy at sea can be identified.

[17] To inspect the time records of the seiche measurements visually, the tidal components and the high-frequency wind waves have been removed from the surface elevation to retain time series in the seiche frequency band (0.1–2.0 mHz). This filtering of the time signal was achieved by Fourier transforming the spectrum in the seiche frequency band back to the time domain. The seiche frequency band was well isolated from the other frequency bands by cosine tapering the original time series (over 10% both at the start and at the end of the signal) before the Fourier transform.

3. Atmospheric Disturbances

3.1. Low-Pressure Weather Systems

[18] With wavelet analysis, a total of 49 seiche events (amplitude exceeding 0.25 m) were identified at Rozenburgse Sluis (ROZ) in the filtered water level signals from January 1995 till December 2001. Meteorological measurements and a visual inspection of the weather charts show that all these events coincided with low-pressure systems with cold fronts crossing the Southern North Sea towards the Dutch coast. However, not all cold fronts moving from sea towards the Dutch coast generated a seiche event. On average approximately one cold front passes the southern North Sea per week and on average seven seiche events occur each year. The fact that most cold fronts do not coincide with significant seiching is ascribed to either the low advection velocity of these systems (inferred from successive weather maps; this situation mainly occurs in summer) or to insufficient strength of these systems (inferred from precipitation radar images).

[19] A review of pertinent meteorological data (weather maps, precipitation radar images and point measurements of atmospheric pressure, wind speed and wind direction) showed two types of cold fronts during seiche events. The first type is sharp with a narrow line of showers (sometimes accompanied by thunder showers, particularly just before the main storm season). Usually, this type of front approaches the coast from a westerly to northwesterly direction. The passage of the front across the harbor coincides with the start of the seiches and it is accompanied by one or more sharp changes ("jumps") in atmospheric pressure and wind direction. The second type of cold front is accompanied by gradual changes in atmospheric pressure and mild precipitation (spread out over a larger area and over a longer time interval, during which the seiche occurs), usually approaching the coast from a northwesterly direction.

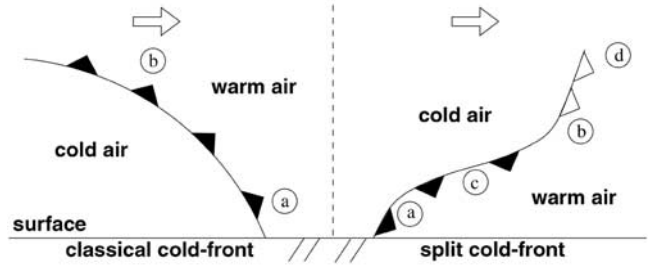

Figure 3. Conceptual cross-sections of the two types of cold fronts (moving from left to right). (left) The classical cold front has one front location at the Earth's surface (circled "a"). At higher altitudes the air rises slowly, which results in less precipitation in that area (circled "b"). (right) The split cold front has a front location at the surface (circled "a") as well as at a higher altitude (circled "b"). The circled "c" indicates the location of the shallow layer of warm air at the surface front. Precipitation is mainly formed near the upper front (circled "d").

3.2. Two Types of Cold Fronts

[20] The above two types of cold fronts have characteristics similar to those of two types of cold front that are conventionally distinguished in meteorology [*Bader et al.*, 1995; *Browning and Monk*, 1982; *Browning*, 1985]. The first is the classical cold front (also called ana cold front or type 1 cold front). It is characterized by sharp changes in atmospheric pressure and wind direction (Figure 3). In this type of front, relatively warm and moist air is forced to ascend rapidly through a column with a width of 2 to 3 km ("a" in Figure 3). This results in a line convection and a narrow line of intense precipitation. In the area behind the front ("b" in Figure 3) the moist air continues to ascend (less rapidly than at the surface front), resulting in mild precipitation.

[21] The second type is the split cold front (also called kata cold front or type 2 cold front). This type of front is characterized by gradual changes in atmospheric pressure, wind speed and wind direction (Figure 3). It can develop from classical cold fronts.

[22] In this type, two fronts occur, one at the Earth's surface ("a" in Figure 3) and one at higher altitudes ("b" in Figure 3); hence the name split front. In this case, dry, cold air is forced to move over a shallow layer of warm moist air ("c" in Figure 3). At the head of this intruding layer of cold air, at an altitude of 3 km to 6 km, warm air is forced to

ascend ("d" in Figure 3). This causes most of the precipitation. The precipitation is more diffuse and less intense compared to the classical cold front.

[23] The above-described types of cold fronts are stereotypical descriptions of extreme situations. Obviously, intermediate situations can be expected and have in fact also been found. During seiche events, gradual cold front situations with scattered precipitation are found as frequently as situations with a broad line of showers near the cold front. Classical cold front situations (with a narrow line of precipitation similar to the situation shown in Figure 7 in section 5.2.1) have been observed during approximately 10 percent of the seiche events.

4. Numerical Simulations

4.1. Governing Equations

[24] Numerical simulations with a hydrodynamic model have been made to investigate the origin of the low-frequency energy at sea. The model solves the continuity equation and the nonlinear momentum balance equation of the water column.

[25] In Cartesian coordinates (x and y) the depth-averaged continuity equation is

$$\frac{\partial h}{\partial t}+\frac{\partial}{\partial x}(u_x D)+\frac{\partial}{\partial y}\left(u_y D\right)=0, \tag{3}$$

in which h is the water level above a reference level, t is time, D is the total water depth, u_x is the depth-averaged velocity in x direction and u_y is the depth-averaged velocity in y direction.

[26] The depth-averaged momentum equation in x direction is

$$\frac{\partial}{\partial t}(u_x D)+\frac{\partial}{\partial x}(u_x u_x D)+\frac{\partial}{\partial y}\left(u_x u_y D\right)=\frac{K_x}{\rho}, \tag{4}$$

in which ρ is the density of water and K_x is the net force per unit area acting on the water column in x direction. The latter term consists of contributions from pressure gradients (atmospheric and hydrostatic), wind stress, bottom friction, horizontal Reynolds stresses (based on eddy viscosity) and Coriolis force. Similar expressions apply to the y direction.

[27] The hydrostatic pressure gradient term and the atmospheric pressure gradient term in x direction are given by, respectively,

$$K_{x,hydrostatic}=-\rho g D\frac{\partial h}{\partial x},\quad K_{x,atmospheric}=-D\frac{\partial p}{\partial x}, \tag{5}$$

in which p is the atmospheric pressure.

[28] The magnitude of the wind shear stress is described by

$$K_{x,wind}=C_d\rho_a U_{10,x}|U_{10}|, \tag{6}$$

in which ρ_a is the density of air, U_{10} is the wind speed at 10 meter elevation, $U_{10,x}$ is the wind speed component in the x direction and C_d is the wind drag coefficient. This drag coefficient is taken to increase linearly from $0.6 * 10^{-3}$ at U_{10} = 0 m/s to a value of $1.95 * 10^{-3}$ at U_{10} = 10 m/s, beyond which it is taken constant.

[29] The magnitude of the shear stress at the bed in x direction is given by

$$K_{x,bed}=-C_b\rho u_x|u|, \tag{7}$$

in which u represents the depth-averaged flow velocity and C_b is a dimensionless shear stress coefficient. C_b is taken to vary with the local depth, resulting in a typical value of $2 * 10^{-3}$ (for D = 30 m).

[30] The lateral Reynolds stresses are described using an eddy viscosity (ν_h). In x direction (and similar in y direction, using u_y instead of u_x) the net force per unit area is

$$K_{x,Reynolds}=-\rho D\nu_h\left(\frac{\partial^2 u_x}{\partial x^2}+\frac{\partial^2 u_x}{\partial y^2}\right). \tag{8}$$

For the simulations described in this study, ν_h = 1 m^2/s is taken (similar to previous calculations based on this model set-up).

4.2. General Description Numerical Model

[31] The hydrodynamic model solves the above described equations on orthogonal, curvilinear, boundary-fitted coordinates (the Delft-3D package, used in a 2D mode for this study) [see, e.g., *Gerritsen et al.*, 2000].

[32] The equations are discretized on a staggered grid: The water level points are defined in the center of a cell, whereas the velocity components are situated at the cell borders. The equations are solved using the alternating direction implicit (ADI) method, in which the time step is split in two. In the first half of the time step, the x derivatives are determined with an implicit numerical scheme, and in the second part of the time step the y derivatives are determined likewise. Both a large-scale model and a nested small-scale model of the (Southern) North Sea including the harbor have been used.

4.3. Grids, Initial Conditions, Boundary Conditions and Driving Forces

[33] For the large-scale simulations, the model set-up for the Southern North Sea of the PROMISE project has been used [*Gerritsen et al.*, 2000], with resolution increasing from 30 km at the northern boundary to 600 m near the harbor mouth (Figure 4). Weakly reflective boundary conditions were applied at the open boundaries, located at the Norwegian Sea in the North and the English Channel in the southwest. These weakly reflective boundary conditions are based on linearized Riemann invariants. These boundary conditions are nonreflective for waves that pass normal to the boundary and reduce reflection in case these are of oblique incidence.

[34] The computations were forced by synthetic fields of atmospheric pressure and wind speed, which were obtained by converting the measured time series of these parameters at a fixed location (at sea or an onshore location near the harbor, depending on the case) into frozen spatial fields. These fields were advected with the velocity of the front (speed and direction), which was inferred from a number of point measurements of atmospheric pressure and, if available, a sequence of precipitation radar images.

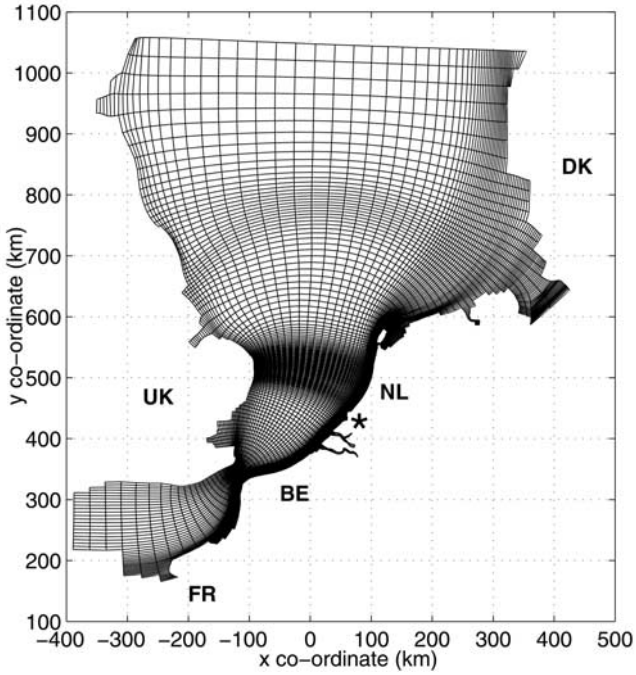

Figure 4. Large-scale computational grid from the PROMISE project. Port of Rotterdam is indicated by the asterisk.

[35] Tides have not been included in the simulations, and all simulations started with an initially undisturbed water level. To assure a gradual start-up of the model, the simulations started with initially slowly changing atmospheric pressure and wind speed. This was achieved by either using the original time series (atmospheric pressure) or by damping the start of the original time series (wind input).

[36] For the small-scale simulations, the model set-up by *Kernkamp* [1999] was used (Figures 5 and 6). This includes

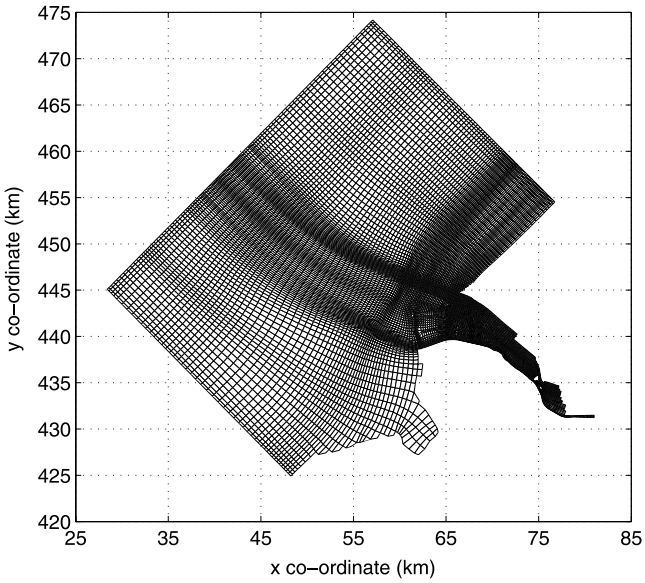

Figure 5. Small-scale, nested computational grid (see details in Figure 6).

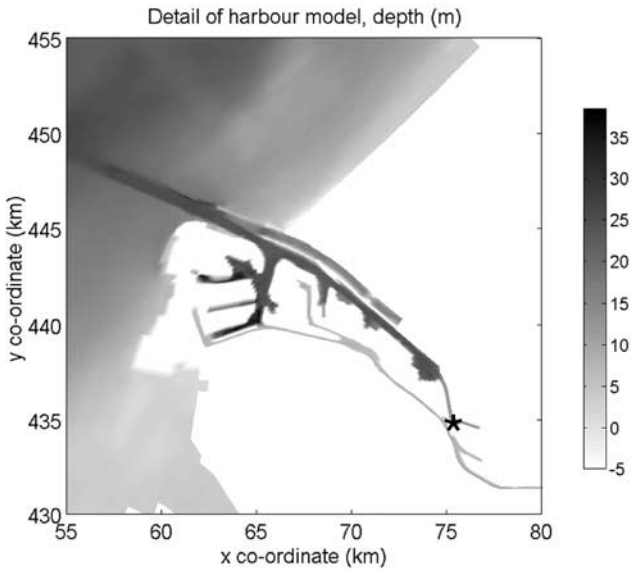

Figure 6. Detail of small-scale computational grid, showing depth values in meters. The location of ROZ is indicated by the asterisk.

the harbor area that is seiche prone (resolution 50 m), together with a small part of the North Sea. These simulations were forced by the results of the large-scale model, which were applied at the open boundaries of the small-scale area as weakly reflective boundary conditions (similar to the type of boundary condition used for the large-scale model).

[37] Preliminary small-scale simulations have been made for the harbor area (without the small North Sea part) with a measured water level near Hook of Holland (Figures 1 and 2) as boundary condition at the harbor mouth. The results from these simulations showed that the model is capable of simulating the observed eigen period at ROZ, although the corresponding seiche amplitudes were overestimated because the water level boundary condition does not allow energy radiation back to sea. A more thorough description of the eigenperiods of parts of the harbor based on this calculation grid has been given by *Kernkamp* [1999].

5. Seiche Events

5.1. Selection of Events

[38] Two seiche events were selected for close analysis and simulation. The first occurred during one of the 35 most severe storms ever recorded by the Royal Netherlands Meteorological Institute (KNMI). A number of publications have been dedicated to this storm, describing the front that occurred in this storm as a typical example of a classical cold front [see, e.g., *Mellink*, 2000]. The second event occurred during a situation with a split cold front (a more "normal" case).

5.2. Seiche With Classical Cold Front

5.2.1. Meteorological Observations

[39] On 30 October 2000 a seiche event occurred that coincided with a classical cold front that passed over the

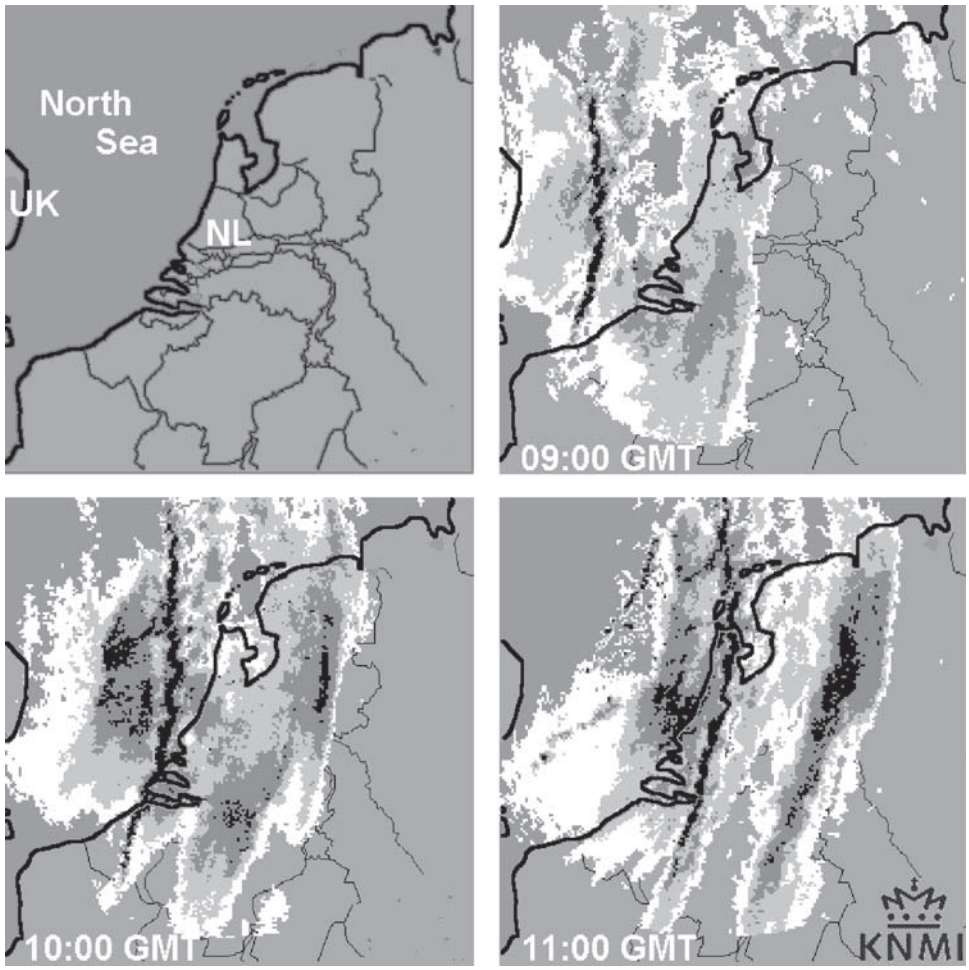

Figure 7. Radar images of precipitation for 30 October 2000 (0900, 1000 and 1100 GMT). The geographic area is shown in the top left image. Gray scales show precipitation intensity from white (mild precipitation) to black (intense precipitation). Images have been edited for clarity in gray scales. Source: Royal Netherlands Meteorological Institute (KNMI).

southern North Sea in an easterly direction. This front showed up as a line of showers (line convection) on precipitation radar images (Figure 7) and as a small jump of approximately 2 hPa in the observed atmospheric pressure.

[40] The left column of Figure 8 depicts the meteorological measurements obtained at Rotterdam Airport for this event. The cold front passage is obvious as a sharp change at 1050 GMT in atmospheric pressure, wind direction, temperature and precipitation.

5.2.2. Measured and Simulated Surface Elevation

[41] The seiche event showed an abrupt increase in amplitude, coinciding with the passage of the cold front (1050 GMT). Subsequently, the amplitude slowly decreased over the next 12 hours (Figure 9). *Rabinovich and Monserrat* [1996] describe this type of seiche as an ''impulse type'': ''strong initial oscillation(s) followed by a fast or slow decay of seiche heights.'' The normalized wavelet spectrum of this seiche event (bottom left panel of Figure 9) shows a peak near the eigenperiod of the harbor near 5400 s.

[42] The right panels of Figure 9 show the surface elevation measurements at sea (EUR) and the corresponding wavelet spectrum. This wavelet spectrum indicates that prior to the seiche, low-frequency energy is found at sea in a narrow band near the eigenperiod of the harbor.

[43] The atmospheric pressure measurements from the different locations at sea were self-similar with only a shift in time. This indicates that the pressure and the wind fields can be reasonably well approximated as moving frozen fields. The front velocity (23 m/s) has been determined from the time lags between the observed jumps in atmospheric pressure at various stations. The direction of movement of the front (from west to east) was inferred from precipitation radar images.

[44] With these rather crude estimates, both the occurrence of the low-frequency energy at sea and the seiche in the harbor are well reproduced as shown by the simulated time series and the corresponding wavelet spectra at sea and in the harbor (EUR and ROZ; compare Figure 10 to Figure 9).

5.3. Seiche With Split Cold Front

5.3.1. Meteorological Observations

[45] On 8 and 9 November 2001 a seiche event occurred that coincided with a weaker cold front that passed over the North Sea in a southerly direction. This front had the characteristics of a split cold front: It did not show sharp

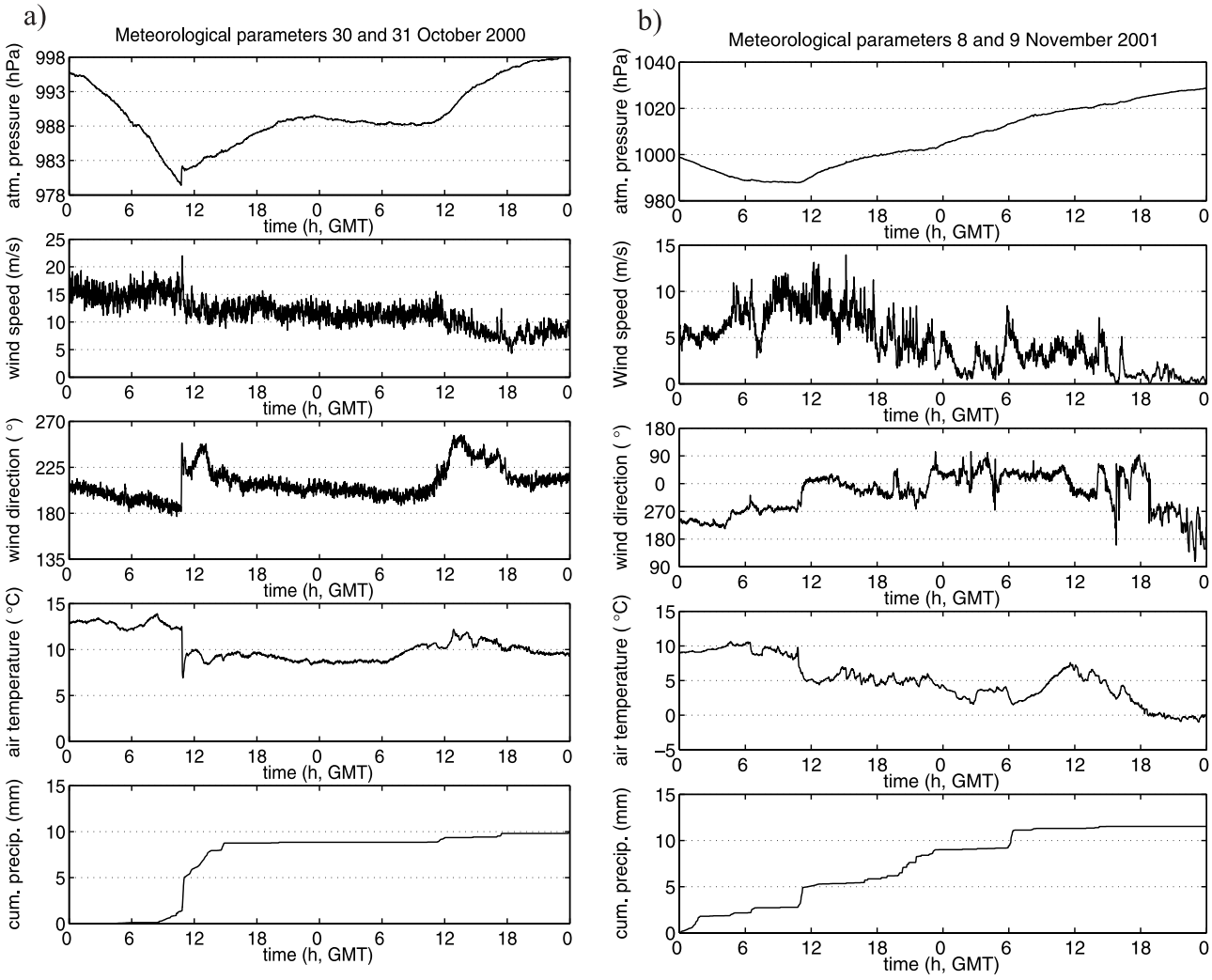

Figure 8. Meteorological observations at Rotterdam Airport (left) during seiche event of 30 October 2000 and (right) during the seiche event of 8 and 9 November 2001. (top to bottom) Atmospheric pressure, wind speed, wind direction, air temperature and cumulative precipitation.

changes in atmospheric pressure and wind direction. The precipitation radar images for these 2 days (not shown here) show that rain was diffuse over a large area. Several local thunderstorms occurred scattered behind the front. The right column of Figure 8 shows the meteorological observations at Rotterdam Airport for this event.

5.3.2. Measured and Simulated Surface Elevation

[46] This seiche event showed alternatingly increasing and decreasing amplitudes with a maximum of approximately 0.5 m (Figure 11). This type of seiche is labeled by *Rabinovich and Monserrat* [1996] as the "complex" type: "a few consecutive abrupt and gradual amplifications and reductions of seiche oscillations." The temperature registration during this event shows a number of sharp changes. The largest temperature drop coincides with the minimum of atmospheric pressure. This corresponds with the passage of the cold front (1050 GMT), which approximately coincides with the start of the event.

[47] The normalized wavelet spectra of the measured surface elevations in the harbor and at sea are shown in Figure 11. The maximum value of the wavelet spectrum for ROZ is found at a period of approximately 6000 s. In contrast with the previous case, here the wavelet spectra are more diffuse, with multiple peaks.

[48] In contrast to the classical cold front situation of 30 October 2000, the atmospheric pressure observations from different locations were not self-similar. The assumption of a moving frozen atmospheric pressure field is therefore a crude approximation at best. This means that a unique direction and speed of the front are not defined. Nevertheless, and for lack of better data, a simulation using the frozen field approach was carried out to investigate its feasibility under these circumstances. The direction of the front was estimated from weather charts, and the velocity of the front was taken from the measured wind velocity at Rotterdam Airport during the passage of the cold front. The frozen pressure and wind fields, based on atmospheric pressure and wind measurements at Rotterdam Airport, were translated in the direction from North to South with a velocity of 12 m/s.

[49] The numerical results (Figure 12) show that the seiche is not well reproduced (compare to Figure 11, note

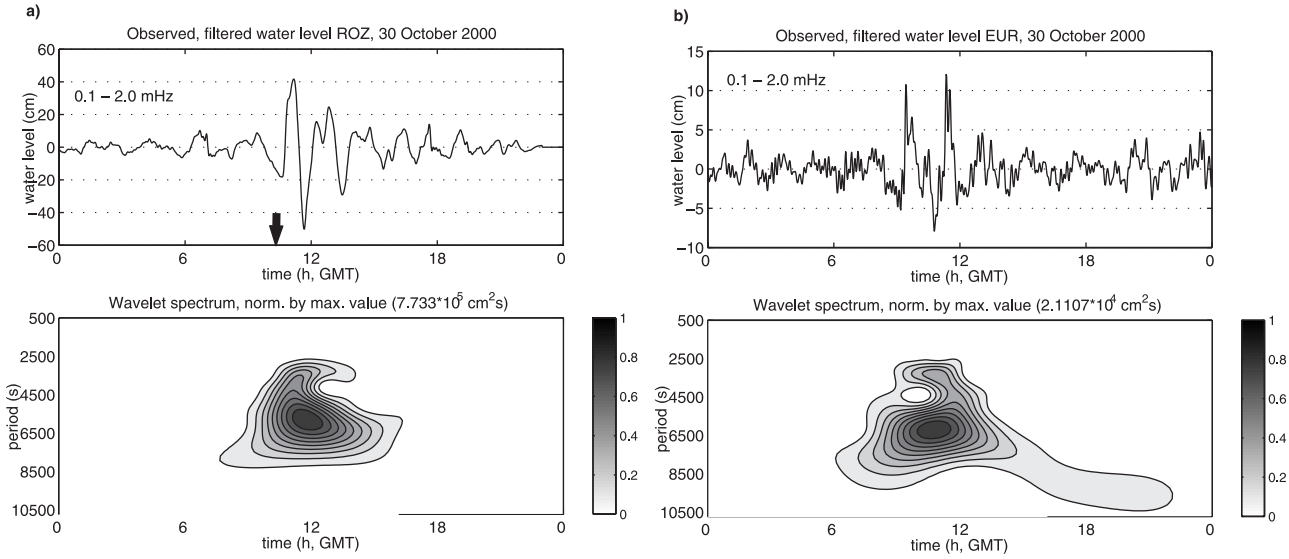

Figure 9. (left) Filtered observed surface elevation at ROZ on 30 October 2000 ((top) Arrow indicates the approximate time of the front passage over the harbor area) and (bottom) the corresponding wavelet spectrum. (right) Filtered observed surface elevation at sea ((top) location EUR, 30 October 2000) and (bottom) the corresponding wavelet spectrum.

the differences in scales). The simulated wavelet spectrum at sea (bottom right panel in Figure 12) shows that energy is generated in the seiche frequency band. The rather erratic behavior of the simulated spectrum resembles that of the observed spectrum, but otherwise the differences are large. The maximum amplitude of the seiche in the simulations is correspondingly poorly estimated: 0.15 m simulated versus 0.5 m observed. The peak period of the simulated seiche is also not correct; the simulated period is 80 min, whereas it is 100 min in the observed spectrum (see bottom left panel in Figure 11). In section 4.3 it was already indicated that the model is capable of reproducing the correct eigenperiods and corresponding seiche amplitudes. This suggests that the incorrect results for the harbor simulation for the gradual case are due to errors in the simulated water levels at sea.

[50] A further analysis of the simulated signals at sea showed that the results were rather sensitive to changes in direction and velocity of the front. A change in direction of 10 degrees counterclockwise resulted in a reduction of the maximum amplitude found in the surface elevation at EUR of 11%. Considering the uncertainty of the estimated front velocity ($\sigma \approx 3$ m/s) simulations were also made with a front velocity of 9 m/s and 15 m/s. In the first case this

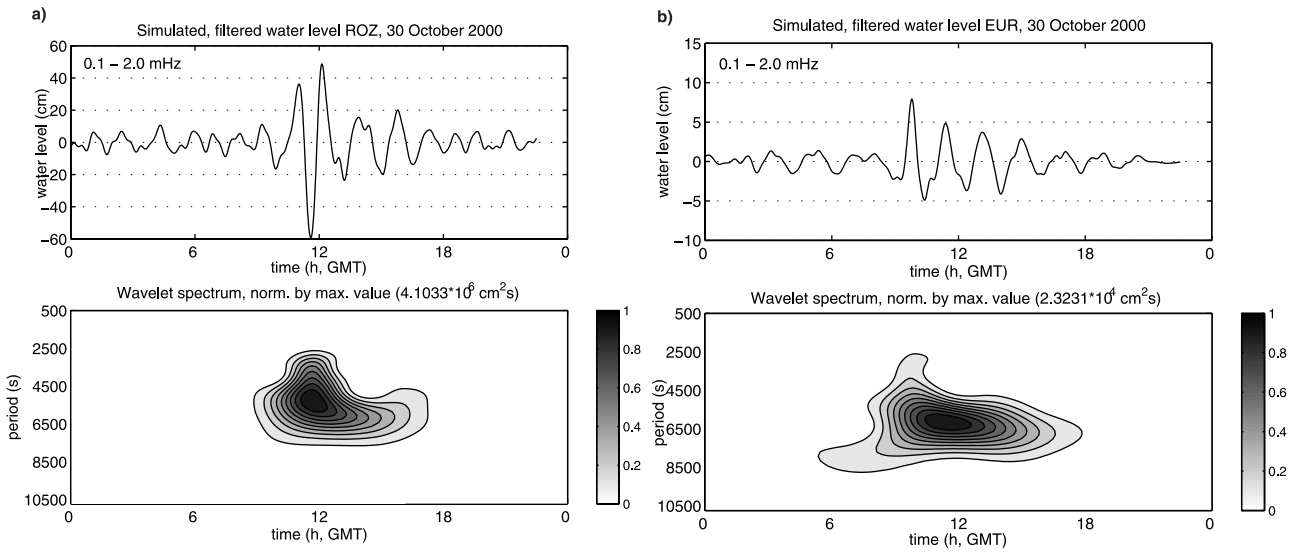

Figure 10. (left) (top) Simulated seiche at ROZ (30 October 2000) and (bottom) the corresponding wavelet spectrum. (right) (top) Simulated water level at EUR (30 October 2000) and (bottom) the corresponding wavelet spectrum.

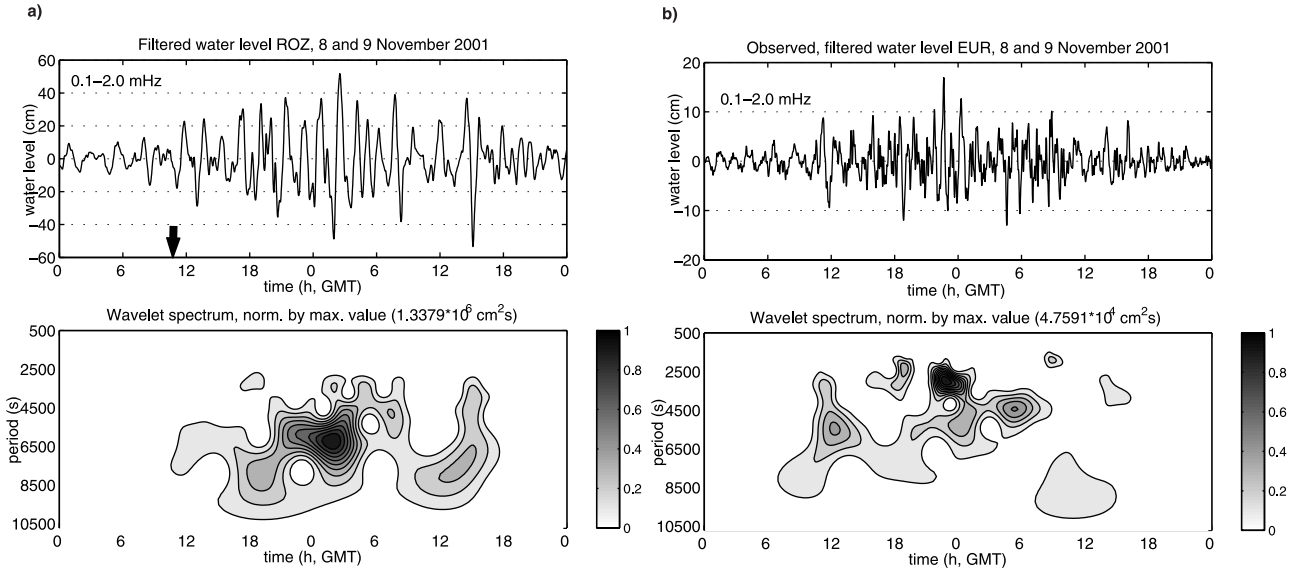

Figure 11. (left) Filtered observed surface elevation measurements at ROZ on 8 and 9 November 2001 ((top) Arrow indicates the approximate time of the front passage over the harbor area) and (bottom) the corresponding wavelet spectrum. (right) (top) Filtered observed surface elevation measurements from EUR (8 and 9 November 2001) and (bottom) the corresponding wavelet spectrum.

resulted in a reduction of the maximum amplitude found at sea (EUR) by 50%, the second case showed a doubling of the maximum amplitude at EUR.

6. Discussion and Conclusions

[51] All seiche events in the Port of Rotterdam in the period of 1995 to 2001 with a maximum amplitude exceeding 0.25 m coincided with the passage of a cold front, some accompanied by thunder showers. They coincided with either a classical cold front with sharp changes in atmospheric pressure and wind direction, or a split cold front with gradual changes of these meteorological parameters. To further investigate seiches coinciding with gradual cold fronts, more observations have been acquired in the winter of 2001–2002.

[52] Measurements at sea showed distinct peaks in wave energy in time and frequency prior to each seiche event. The corresponding wavelet spectra were narrow-banded compared to the full seiche frequency band (0.1–2.0 mHz).

[53] Computations with a numerical hydrodynamic model forced by fields of atmospheric pressure and wind, based on observations from a location at sea, correctly reproduced the generation of low-frequency energy at sea by the classical

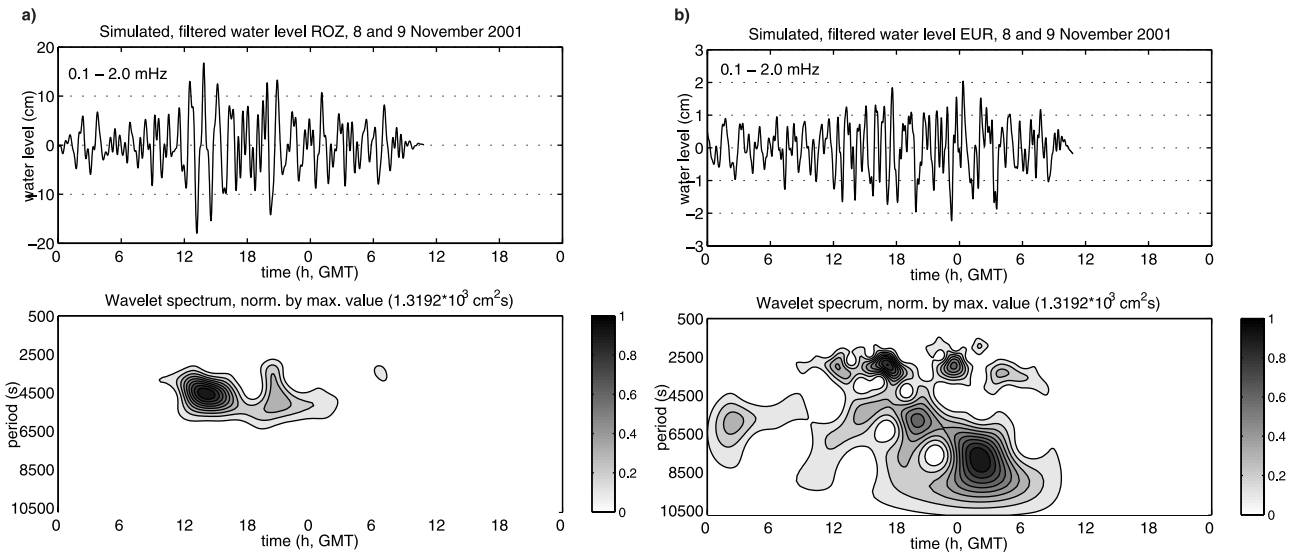

Figure 12. (left) (top) Simulated water level from ROZ (8 and 9 November 2001) and (bottom) the corresponding wavelet spectrum. (right) (top) Simulated water level from EUR (8 and 9 November 2001) and (bottom) the corresponding wavelet spectrum.

cold front and the occurrence of a seiche event in the Port of Rotterdam with the correct amplitude. On the other hand, the numerical simulations for the split cold front could not correctly reproduce the low-frequency energy at sea and, therefore, also failed to reproduce the seiche event in the harbor. These incorrect results for the split cold front situation are ascribed to errors in the forcing of the large-scale model. The characteristics of the split-front situations indicate that (contrary to the classical cold front situations) they do not lend themselves to being approximated by frozen pressure and wind fields. The errors that can be introduced by the use of frozen fields for these cases are also illustrated by the large sensitivity of the results for the estimated parameters of these fields (direction and speed). Therefore, the driving forces in future simulations will be taken from a high-resolution (2 km) dynamical numerical meteorological model (that has only recently become available as an experimental version) instead of the synthetic, frozen fields of the present study. It is hoped that these high-resolution meteorological model results will introduce the relevant time and length scales. In any case, errors introduced by using an estimated constant direction and speed of the meteorological system (especially for the gradual cold fronts) will then be avoided.

[54] **Acknowledgments.** The first author (M.P.C.de J.) acknowledges the financial support of the Dr. Ir. Cornelis Lely Foundation and of the Directorate-General for Public Works and Water Management (RWS). Furthermore, the authors thank J. Rozema and M. van Dijk of the North Sea Directorate of RWS for providing the measurement data at sea. The authors also thank C. Mooiman, R. Kamphuis and N. van Neerven of the Rotterdam Municipal Port Management for providing them with the measurements from the Port of Rotterdam. In addition, the authors thank the Royal Netherlands Meteorological Institute (KNMI) for the meteorological measurements, weather maps and precipitation images, in particular P. van Es (KNMI) for the meteorological measurements from Rotterdam Airport. The authors thank WL | Delft Hydraulics for putting the Delft 3D simulation package at their disposal and for permission to use its curvilinear EU/PROMISE and harbor (Europoort) model set-up. Wavelet software was provided by C. Torrence and G. Compo [*Torrence and Compo*, 1998] (available through http://paos.colorado.edu/research/wavelets/).

References

Bader, M., G. S. Forbes, J. R. Grant, R. B. E. Rilley, and A. J. Waters, *Images in Weather Forecasting: A Practical Guide for Interpreting Satellite and Radar Imagery*, Cambridge Univ. Press, New York, 1995.

Browning, K. A., Conceptual models of precipitation systems, *Meteorol. Mag.*, *114*(1359), 293–319, 1985.

Browning, K. A., and G. A. Monk, A simple model for the synoptic analysis of cold fronts, *Q. J. R. Meteorol. Soc.*, *108*, 435–452, 1982.

Candela, J., S. Mazzola, C. Sammari, R. Limeburner, C. J. Lozano, B. Patti, and A. Bonnano, The "mad sea" phenomenon in the Strait of Sicily, *J. Phys. Oceanogr.*, *29*(9), 2210–2231, 1999.

de Looff, H., and J. J. Veldman, Seiches in the Port of Rotterdam during storm surges, paper presented at International Symposium: Waves-Physical and Numerical Modelling, Am. Soc. of Civ. Eng., Vancouver, Canada, 1994.

Farge, M., Wavelet transforms and their applications to turbulence, *Annual Rev.*, *1992*, 395–457, 1992.

Garcies, M., D. Gomis, and S. Monserrat, Pressure-forced seiches of large amplitude in inlets of the Balearic Islands: 2. Observational study, *J. Geophys. Res.*, *101*(C3), 6453–6467, 1996.

Gerritsen, H., R. J. Vos, T. van der Kaaij, A. Lane, and J. G. Boon, Suspended sediment modelling in a shelf sea (North Sea), *Coastal Eng.*, *41*(1–3), 317–352, 2000.

Giese, G. S., and D. C. Chapman, Coastal seiches, *Oceanus*, *36*(1), 38–46, 1993.

Gomis, D., S. Monserrat, and J. Tintoré, Pressure-forced seiches of large amplitude in inlets of the Balearic Islands, *J. Geophys. Res.*, *98*(C8), 14,437–14,445, 1993.

Hibiya, T., and K. Kajiura, Origin of the Abiki phenomenon (a kind of seiche) in Nagasaki Bay, *J. Oceaonogr. Soc. Japn.*, *38*, 172–182, 1982.

Kernkamp, H. W. J., Seiches Europoort-Continuation of seiche calculations Maasvlakte 2 alternatives (in Dutch), *Tech. Rep. Z2635*, WL | Delft Hydraulics, 1999.

Korgen, B. J., Seiches, transient standing-wave oscillations in water bodies can create hazards to navigation and unexpected changes in water conditions, *Am. Sci.*, *83*, 330–341, 1995.

Mei, C. C., *The Applied Dynamics of Ocean Surface Waves*, John Wiley, New York, 1989.

Mellink, H., The severe storm of 30 October 2000: Radar images show meso-scale structures (in Dutch), *Metorologica*, *4*(9), 30–31, 2000.

Monserrat, S., A. Ibbetson, and A. J. Thorpe, Atmospheric gravity waves and the 'rissaga' phenomenon, *Q. J. R. Meteorol. Soc.*, *117*, 553–570, 1991a.

Monserrat, S., C. Ramis, and A. J. Thorpe, Large-amplitude pressure oscillations in the western Mediterranean, *Geophys. Res. Lett.*, *18*(2), 183–186, 1991b.

Morlet, J., G. Arens, E. Furgeau, and D. Giard, Wave propagation and sampling Theory: 2, Sampling theory and complex waves, *Geophysics*, *47*(2), 222–236, 1982.

Rabinovich, A. B., and S. Monserrat, Meteorological tsunamis near the Balearic and Kuril Islands: Descriptive and statistical analysis, *Nat. Hazards*, *13*(1), 55–90, 1996.

Rabinovich, A. B., and S. Monserrat, Generation of meteorological tsunamis (large amplitude seiches) near the Balearic and Kuril islands, *Nat. Hazards*, *18*, 27–55, 1998.

Torrence, C., and G. P. Compo, A practical guide to wavelet analysis, *Bull. Am. Meteorol. Soc.*, *79*, 61–78, 1998.

Vidal, C., R. Medina, S. Monserrat, and F. L. Matín, Harbor resonance induced by pressure-forced surface waves, paper presented at Coastal Engineering 2000 (ICCE 2000), Am. Soc. of Civ. Eng., Reston, Va., 2001.

Wemelsfelder, P. J., Origin and effects of long period waves in ports, paper presented at Congres International des Navigation, Int. Navig. Assoc., Brussels, Belgium, 1957.

Wilson, B. W., Seiches, *Adv. Hydrosci*, *8*, 1–94, 1972.

J. A. Battjes, M. P. C. de Jong, and L. H. Holthuijsen, Environmental Fluid Mechanics Section, Delft University of Technology, P.O. Box 5048, 2600 GA, Delft, Netherlands. (j.battjes@ct.tudelft.nl; m.p.c.dejong@ct.tudelft.nl; l.h.holthuijsen@ct.tudelft.nl)